ACS Sustainable Chemistry & Engineering

Research Article

Cite This: ACS Sustainable Chem. Eng. 2018, 6, 13907−13914

pubs.acs.org/journal/ascecg

Effective Zinc Adsorption Driven by Electrochemical Redox Reactions of Birnessite Nanosheets Generated by Solar Photochemistry

Lihu Liu,[†] Wenfeng Tan,[†] Steven L. Suib,[‡] Guohong Qiu,*[,†] Lirong Zheng,[§] Qiaoyun Huang,[†] and Chengshuai Liu[∥]

[†]Key Laboratory of Arable Land Conservation (Middle and Lower Reaches of Yangtse River), Ministry of Agriculture, Hubei Key Laboratory of Soil Environment and Pollution Remediation, College of Resources and Environment, Huazhong Agricultural University, Wuhan 430070, Hubei Province China

[‡]Department of Chemistry, University of Connecticut, 55 North Eagleville Road, Storrs, Connecticut 06269-3060, United States

[§]Beijing Synchrotron Radiation Facility, Institute of High Energy Physics, Chinese Academy of Sciences, Beijing 100039, China

[∥]State Key Laboratory of Environmental Geochemistry, Institute of Geochemistry, Chinese Academy of Sciences, Guiyang 550081, China

Supporting Information

ABSTRACT: The surface properties, chemical compositions, and crystal structures of manganese oxides can be altered by redox reactions, which affect their heavy metal ion adsorption capacities. Here, birnessite nanosheets (δ-MnO_2) were synthesized from the photochemical reaction of Mn^{2+}_{aq} and nitrate under solar irradiation, and Zn^{2+} was electrochemically adsorbed using the as-obtained birnessite nanosheets by galvanostatic charge−discharge. The effects of current density and electrochemical techniques (symmetric electrode and three-electrode systems) on Zn^{2+} adsorption capacity were also investigated. The results showed that the maximum Zn^{2+} adsorption capacity of the birnessite in the presence of electrochemical redox reactions could reach 383.2 mg g^{-1} (589.0 mmol mol^{-1}) and 442.6 mg g^{-1} (680.3 mmol mol^{-1}) in the symmetric electrode and three-electrode system, respectively; however, the Mn^{2+} release capacity in the three-electrode system was higher than that in the symmetric electrode system. With increasing current density, the Zn^{2+} adsorption capacity decreased. In addition, the system for heavy metal ion removal driven by electrochemical redox reactions could also be used as a supercapacitor for power storage. The present work proposes a "green" and sustainable approach for preparing nanosized birnessite, and it clarifies the adsorption mechanism of birnessite for Zn^{2+} in the presence of electrochemical redox reactions.

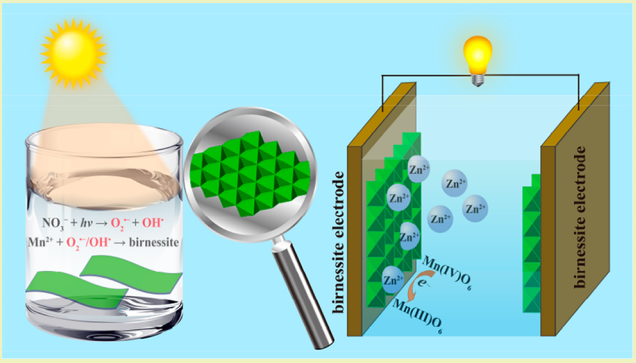

KEYWORDS: *nitrate photolysis, solar energy, birnessite nanosheets, electrochemical adsorption, heavy metal ions, Zn^{2+}*

INTRODUCTION

Large amounts of heavy metal ions have been discharged into the environment with the rapid growth of industries. Many of these ions are toxic, and can accumulate in living organisms and thus cause serious health problems.[1,2] Zinc, a common heavy metal ion in the wastewater discharged from industries, is toxic when the concentration exceeds the allowable limit.[3] In addition, Zn contamination can hinder plant growth.[4] Accordingly, different methods for removing heavy metal ions from wastewaters have been developed. The applications of membrane filtration and ion-exchange methods are limited because of the difficulties in regenerating membrane and resin and the high cost, although the two methods are highly efficient and rapid.[1,5] Chemical precipitation is widely used for its relatively easier operation and lower cost, but it is less efficient for the wastewater containing complexing agents or low-concentration heavy metal ions. Adsorption has advantages in both operation and cost and thus is considered as a cost-effective strategy.[1,2]

Manganese oxides have widespread applications in the adsorption for heavy metal ions because of their properties of low point of zero charge, eco-friendliness, and abundant resources.[6−8] The adsorption capacities of manganese oxides for heavy metal ions are different owing to their various properties including crystal structure, adsorption site, specific surface area, and micromorphology. Generally, the adsorption

Received: May 13, 2018
Revised: October 5, 2018
Published: October 8, 2018

DOI: 10.1021/acssuschemeng.8b02191
ACS Sustainable Chem. Eng. 2018, 6, 13907−13914

capacities for Zn^{2+}, Pb^{2+}, and Cd^{2+} follow the order of birnessite > cryptomelane > todorokite > hausmannite.[9] In addition, the same type of manganese oxides with different Mn AOS are different in heavy metal ion adsorption capacities.[10] Thus, during the adsorption process, the adsorption capacity of manganese oxide for heavy metal ions may be improved through adjusting the properties including chemical composition and Mn AOS.

Heavy metal ions are mainly coordinated with O in the MnO_6 octahedra of manganese oxides to form inner-sphere complexes, and redox reactions are seldom considered in the isothermal adsorption.[9,10] Our previous work showed that the Mn AOS and micromorphology of manganese oxide were altered during electrochemical redox reactions.[11] Manganese oxides are also widely used in deionization capacitors to improve the adsorption performance for salt[12,13] and heavy metal[14] ions; however, the enhancement of adsorption capacities is sometimes assigned to the polarization potential and special structure of electrode materials.[12,13] The effect of electrochemically controlled redox reactions of manganese oxides on their heavy metal ion adsorption capacities remains elusive.

Hexagonal birnessite is composed of edge-sharing MnO_6 octahedral layers, and the Mn(IV) vacancies in the layers are considered as strong adsorption sites for heavy metal ions.[6,15,16] In our previous work, birnessite obtained through the reduction of $KMnO_4$ was used as electrode materials. In the three-electrode system, the adsorption capacities of birnessite was 530.0 mg g^{-1} for Zn^{2+} and 900.7 mg g^{-1} for Cd^{2+} using galvanostatic charge−discharge. Meanwhile, the effects of cycle number and pH were also investigated. However, up to one-third of Mn was released into the solution from the birnessite electrode during the adsorption process.[8,17] Further investigations are needed to clarify the adsorption mechanism and reduce the release of Mn^{2+}.

Hexagonal birnessite is usually prepared through reflux,[10,18] hydrothermal,[19] or sol−gel[7] methods in laboratory. However, most of these methods require heat energy, high pressure, or complex operation.[20] In addition, with increasing environmental pollution, the current methods for preparing nanomaterials need to be re-evaluated from the perspectives of pollution, energy consumption, and waste production.[21] Photochemical methods, especially those using solar energy, are considered as "green" and sustainable approaches because of their low energy consumption and less waste production.[21,22] As a common photocatalyst, NO_3^- can produce ROS including hydroxyl ($OH^\bullet$) and superoxide ($O_2^{\bullet-}$) radicals under ultraviolet (UV) irradiation,[23,24] which will oxidize low-valence ions such as Mn^{2+}_{aq} and Fe^{2+}_{aq} to high-valence oxides or ions.[23] As previously reported, δ-MnO_2 was generated in the photochemical reaction of Mn^{2+}_{aq} and NO_3^-, and $O_2^{\bullet-}$ rather than $OH^\bullet$ is regarded as the main oxidant.[20] The unique micromorphology of the photochemical synthesized birnessite may facilitate the electrochemical adsorption for heavy metal ions. Our previous work has indicated that $OH^\bullet$ contributes to the oxidation of Fe^{2+} to iron oxide nanominerals.[25] Hence, the effect of $OH^\bullet$ formed from NO_3^- photolysis on the formation of birnessite under solar irradiation needs further elucidation.

Here, birnessite nanosheets were obtained through the photocatalytic oxidation of Mn^{2+}_{aq}, and the synthesized birnessite nanosheets were used for Zn^{2+} removal in the presence of electrochemical redox reactions. The effects of current density and electrochemical techniques (symmetric electrode and three-electrode systems) on the adsorption performance of the birnessite nanosheets were also investigated. This work elucidates the electrochemical adsorption mechanism of birnessite for Zn^{2+} and provides a facile method for heavy mental ion removal from aqueous solution.

EXPERIMENTAL SECTION

Photochemical Synthesis of Birnessite Nanosheets. Birnessite nanosheets were fabricated by a photochemical method.[20] A mixed solution containing $NaNO_3$ and $MnSO_4$ was prepared, and their concentrations were controlled at 200 and 10.0 mmol L^{-1}, respectively. A NaOH solution at the concentration of 0.1 mol L^{-1} was added to adjust the initial pH to 8.0. Then, the solution was poured into 150 mL quartz tubes with a volume of 100 mL in each tube. These quartz tubes were sealed and transferred to the rooftop (30.476111°N, 114.353333°E) under solar irradiation. The experiments were conducted from 10:00 to 16:00 during August 15−20, 2016, and the air temperature varied between 23 to 38 °C. The intensity of solar light was determined to be from 0.24 to 1.78 mW cm^{-2} by a UV-A irradiatometer (Photoelectric Instrument Factory of Beijing Normal University) at 320−400 nm. Only the intensity of solar light between 320−400 nm was determined because of the excitation band of nitrate and detection limitation of irradiatometer in our lab (Supporting Information). The photochemical reaction of $NaNO_3$ (0.2 mmol L^{-1}) and $MnSO_4$ (0.1 mmol L^{-1}) with a constant pH of 6.0 (controlled by acetic acid/sodium acetate (5 mmol L^{-1}) buffer) was also performed to investigate the possibility of the photochemical reaction in natural environments. The resulting precipitate was filtered and washed, and then dried at 40 °C overnight.

Electrochemically Controlled Adsorption of Zinc. The electrochemical adsorption of Zn^{2+} was performed in symmetric electrode and three-electrode system with 30 mL Zn-containing solution by charge−discharge for 50 cycles at room temperature on a CT-3008W-5V5mA battery testing system. Detailed electrode preparations are presented in the Supporting Information. Na_2SO_4 (0.1 mol L^{-1}) and $ZnSO_4$ were used to prepare Zn-containing solutions with the initial Zn^{2+} concentration of 0 to 1800 mg L^{-1}. $NaOH/H_2SO_4$ solution at the concentration of 0.1 mol L^{-1} was added to adjust the initial pH of these solutions to 5.0. In the symmetric electrode system, the current density of charge−discharge was controlled to be from 0.1 to 0.5 A g^{-1}, and the potential of charge−discharge was controlled to be from −0.9 to +0.9 V. In the three-electrode system, the current density of charge−discharge was controlled at 0.1 A g^{-1}, and the potential (vs SCE) of charge−discharge was controlled to be from 0 to +0.9 V. The electrodes were washed to remove the Zn-containing solution after multicycle redox reactions and then characterized by power X-ray diffraction (XRD) before drying at 60 °C under vacuum.

The electrochemical specific capacitance C_m (F g^{-1}) and Zn^{2+} adsorption capacity Q_s (mg g^{-1}) were respectively calculated according to eq 1[26] and eq 2:[14]

$$C_m = \frac{4I\Delta t}{m\Delta V} \quad (1)$$

$$Q_s = \frac{(C_0 - C_s)V_s}{m} \quad (2)$$

In the equations, Δt, I, and ΔV, respectively, represent the discharge time, current, and potential range; m represents the birnessite mass on the working electrode and counter electrode; C_0 and C_s, respectively, represent the Zn^{2+} concentration in the initial reaction system and after electrochemical adsorption; and V_s represents the volume of Zn-containing solution.

Analytical Methods. XRD characterization was performed on a D8 ADVANCE diffractometer (Bruker) with Cu Kα radiation. Analyses of Fourier-transform infrared (FT-IR) spectra were conducted on a VERTEX 70 spectrometer (Bruker). Field emission scanning electron microscopy (FESEM, SU8000, Hitachi) was used

DOI: 10.1021/acssuschemeng.8b02191
ACS Sustainable Chem. Eng. 2018, 6, 13907−13914

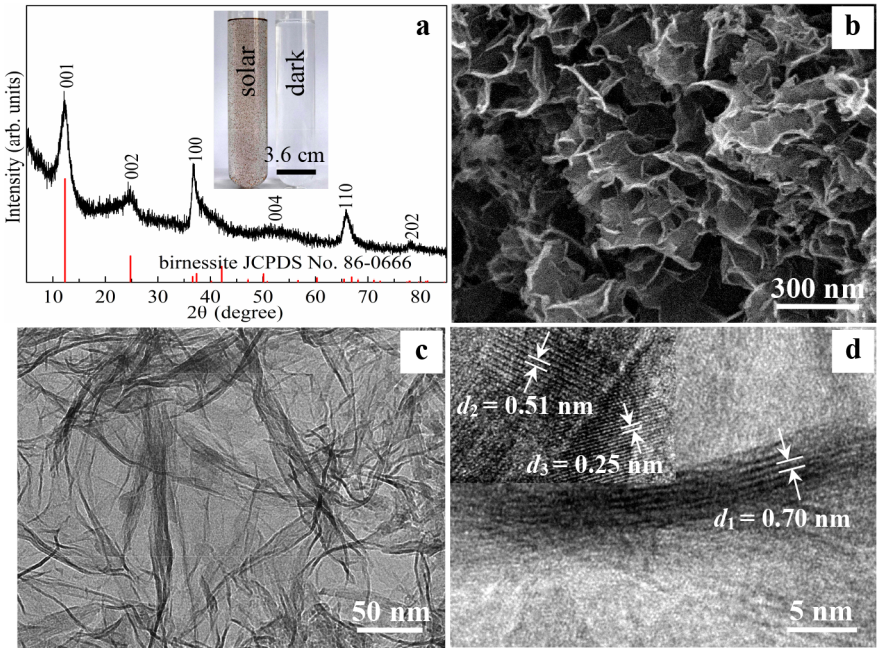

Figure 1. XRD pattern and photograph (a), FESEM (b), TEM (c) and HRTEM images (d) of the birnessite formed under solar irradiation in aqueous reaction system of $NaNO_3$ (200 mmol L^{-1}) and $MnSO_4$ (10 mmol L^{-1}) with the initial pH of 8.0 for 6 h. The photograph under dark conditions was also presented in (a).

to observe the micromorphology. Transmission electron microscopy (TEM) analyses were conducted using Talos F200C (FEI). The ASAP 2020 (Micromeritics) was used to analyze the pore property and specific surface area. The BJH (Barrett–Joyner–Halenda) method was applied for the calculation of pore sizes.[27] The proportions of Mn with different valences were analyzed by X-ray absorption near-edge structure (XANES) spectra collected at the Beijing Synchrotron Radiation Facility (1W1B beamline), China. The collection and analysis of XANES spectra are shown in the Supporting Information. To examine the existence of $O_2^{\bullet-}$ and $OH^{\bullet}$, superoxide dismutase (SOD)[20] (10 mg L^{-1}) and benzoate (BA)[28] (0.4 mmol L^{-1}) were, respectively, added into the reaction of $NaNO_3$ (0.2 mmol L^{-1}) and $MnSO_4$ (0.1 mmol L^{-1}) with the initial pH of 6.0 under solar irradiation. An atomic absorption spectrometer (AAS240FS) was used to determine the concentrations of Zn^{2+} and Mn^{2+}. A CHI660E electrochemical workstation was used to collect the cyclic voltammetry plots. The scan rate and range were 0.5 mV s^{-1} and −0.9 to +0.9 V, respectively.

RESULTS

Preparation of Birnessite Nanosheets. The photograph of the solids formed in the photochemical reaction was shown in Figure 1a. Dark brown precipitates were formed in the mixed solution of $MnSO_4$ and $NaNO_3$ under solar irradiation for 6 h, while no solid product was generated under dark conditions. The XRD pattern and FT-IR spectra of the solid product formed under solar irradiation indicated the generation of single-phase birnessite (JCPDS card no. 86-0666) (Figure 1a and Figure S1). The ratio of d_{100} to d_{110} in XRD pattern was close to $\sqrt{3}$, indicating the formation of hexagonal birnessite.[29,30]

The FESEM and TEM images indicated that uniform sheet-like birnessite was generated in the photochemical reaction (Figure 1b,c). The corresponding HRTEM images exhibited the (001) and (100) planes with an average interplanar spacing of 0.70 and 0.25 nm (Figure 1d), respectively. The occur of average interlayer spacing of 0.51 nm was possibly due to the collapse of birnessite interlayers by dehydration in TEM sample chamber with high vacuum, which was also observed in triclinic birnessite.[31] The N_2 adsorption–desorption isotherm of the birnessite showed type-IV isotherm and H_3-type hysteresis (Figure S2a).[27] The two-dimensional birnessite had a BET specific surface area of 179 m^2 g^{-1}, which was comparable to that of δ-MnO_2 nanoparticles obtained from the comproportionation of $KMnO_4$ and Mn^{2+}_{aq}.[18] The total pore volume and average pore diameter obtained using the BJH method were 0.67 cm^3 g^{-1} and 15.5 nm, respectively (Figure S2b).

Zinc Adsorption Driven by Electrochemical Redox Reactions. Figure 2 shows the cyclic voltammetry plots of

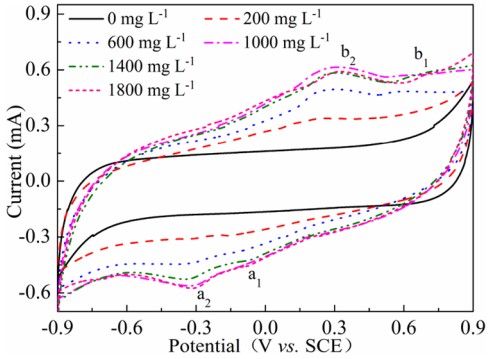

Figure 2. First-cycle cyclic voltammetry plots of the birnessite electrodes in symmetric electrode system at a scan rate of 0.5 mV s^{-1} in Zn^{2+} solutions with different concentrations.

birnessite electrodes for the first cycle in the symmetric electrode system in Zn^{2+} solutions at different concentrations. In the Na_2SO_4 solution without Zn^{2+}, a relatively rectangular shape was observed, suggesting that the redox reaction of birnessite electrode was reversible. In the presence of Zn^{2+}, two pairs of redox peaks and asymmetrical cyclic voltammetry plots were obtained. With increasing Zn^{2+} concentration, the

DOI: 10.1021/acssuschemeng.8b02191
ACS Sustainable Chem. Eng. 2018, 6, 13907−13914

asymmetrical degree and redox current first increased and subsequently reached the maximum. In Zn/MnO_2 batteries, the insertion−extraction process of Zn^{2+} takes place during the redox reactions of Mn(II/III) and Mn(IV).[32,33] In this work, the peak a_1/b_1 can be assigned to the insertion/extraction of Zn^{2+} on the surface of the birnessite, the peak a_2/b_2 can be assigned to the reduction/oxidation of Mn(IV) and Mn(II/III). The asymmetrical redox peaks and cyclic voltammetry plots demonstrated the incomplete reversibility of the redox reactions of Mn(IV) and Mn(II/III).

Figure 3 shows the Zn^{2+} adsorption capacities of birnessite electrodes in the symmetric electrode system after 50 cycles of

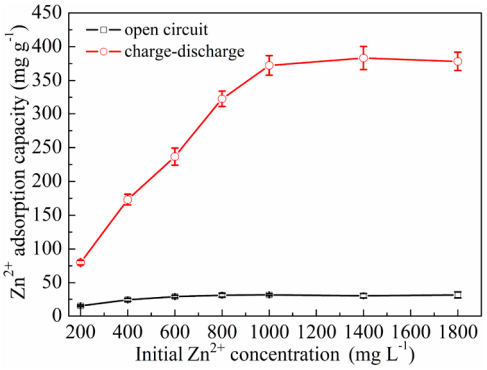

Figure 3. Zn^{2+} adsorption capacities of the birnessite electrodes in symmetric electrode system after charge−discharge for 50 cycles and at open circuit for 12 h in Zn^{2+} solutions with different concentrations.

redox reaction and at open circuit in Zn^{2+} solutions at different concentrations. The Zn^{2+} adsorption capacity was 79.9 mg g^{-1} (122.8 mmol mol^{-1}) in 200 mg L^{-1} Zn^{2+} solution, and then increased with increasing Zn^{2+} concentration. The maximum Zn^{2+} adsorption capacity of birnessite electrode was, respectively, 31.5 mg g^{-1} (48.4 mmol mol^{-1}) and 383.2 mg g^{-1} (589.0 mmol mol^{-1}) at open circuit and after charge−discharge. The adsorption capacities of different materials for Zn^{2+} are presented in Table S1. The Zn^{2+} adsorption capacity of birnessite with electrochemical redox reactions was higher than the isothermal adsorption capacities of these adsorbents. The corresponding Mn^{2+} release from birnessite electrode increased with increasing Zn^{2+} adsorption capacity, and the highest release capacity was 54.0 and 112.2 mg g^{-1} at open circuit and after charge−discharge, respectively (Figure S3). The final pH of the solution after electrochemical redox reactions increased from 4.51 to 5.79 with the initial Zn^{2+} concentration increasing from 200 to 1800 mg L^{-1}.

XRD, XANES, and FESEM were used to characterize the intermediate products in the electrochemical adsorption of Zn^{2+}. The XRD patterns of the working electrode in symmetric electrode system after 50 cycles of redox reaction in Zn^{2+} solutions at different concentrations indicated that no new phase was formed (Figure 4a). In the study of the effect of Mn AOS on the d_{110} value of birnessite and Pb-adsorbed birnessite, it was claimed that the number of Mn(IV) vacancies increased with increasing Mn AOS, which would lead to an increase in the electrostatic repulsion between adjacent cations around Mn(IV) vacancies and a decrease in d_{110} value.[34−36] Therefore, we speculate that the Mn AOS probably decreased, as indicated by the slight increase in the d_{110} value with the increase of Zn^{2+} concentration (Figure 4b). The crystal

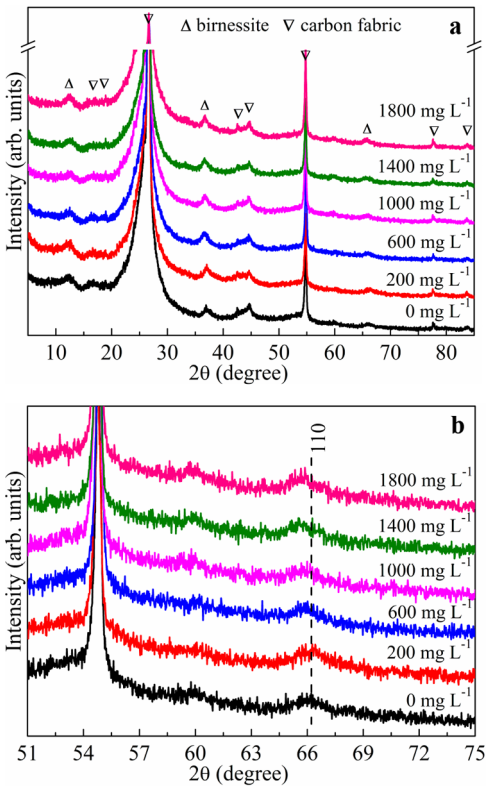

Figure 4. XRD (a) and the corresponding magnified patterns (b) of the working electrodes in symmetric electrode system after charge−discharge for 50 cycles in Zn^{2+} solutions with different concentrations.

structure of birnessite changed little at open circuit as indicated by the XRD patterns (Figure S4).

The Combo method was used to further clarify the Mn AOS from the Mn K-edge XANES derivative spectra of the birnessite electrodes after redox reactions (Figure 5 and

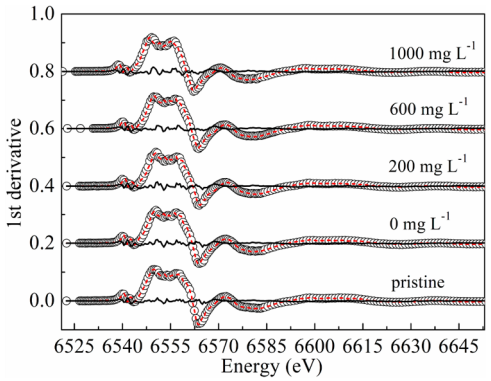

Figure 5. Linear combination fits of the Mn K-edge XANES derivative spectra for the working electrodes in symmetric electrode system of Zn^{2+} solutions at different concentrations. Open circles are the first derivative spectra, dashed lines are the best-fitted curves, and solid lines are the residuals.

Table S2).[37] Table S2 presents the standard samples used in the fitting process. The Mn AOS was 3.43 in the as-obtained birnessite. With increasing Zn^{2+} concentration, the Mn(IV) and Mn(III) proportion, respectively, decreased and increased in the birnessite electrode after electrochemical adsorption. The Mn AOS values in the birnessite electrodes were

DOI: 10.1021/acssuschemeng.8b02191
ACS Sustainable Chem. Eng. 2018, 6, 13907−13914

respectively 3.51, 3.45, 3.42, and 3.40 after electrochemical adsorption in 0, 200, 600, and 1000 mg L^{-1} Zn^{2+} solutions. Although the accuracy of the Mn AOS is about 0.04 valence units obtained from the Combo method,[37] it showed a downward trend with increasing Zn^{2+} concentration, which was consistent with the change of d_{110} value in the XRD results (Figure 4b). These results further demonstrated the incomplete reversibility of redox reactions of birnessite during the electrochemical adsorption.

Figure S5 shows the FESEM images of the birnessite electrode after electrochemical redox reactions. In the Na_2SO_4 solution without Zn^{2+}, the micromorphology of birnessite was altered from nanosheets to nanoparticles. The nanosheets gradually disappeared, and cross-linked networks were formed with increasing Zn^{2+} concentration, further suggesting the changes in the micromorphology of birnessite during the electrochemical oxidation−reduction.

Effects of Rate and Degree of Redox Reactions on Zn^{2+} Adsorption. The redox rate of birnessite can be adjusted by changing the current density, which affects the electrochemical adsorption capacity. Figure S6 shows the electrochemical specific capacitance of birnessite electrode in the symmetric electrode system at different current densities in 200 mg L^{-1} Zn^{2+} solution. The electrochemical specific capacitance showed a decreasing trend with increasing current density. Figure 6 shows the Zn^{2+} adsorption capacity of birnessite electrode after electrochemical redox reactions in the symmetric electrode system at different current densities. The Zn^{2+} adsorption capacity and Mn^{2+} release capacity were, respectively, 29.0 and 45.0 mg g^{-1} when the current density was controlled at 0.5 A g^{-1}. With decreasing current density, the Zn^{2+} adsorption capacity and Mn^{2+} release capacity, respectively, increased and decreased (Figure 6a and Figure S7). The XRD patterns indicated that no new phase was formed during the electrochemical redox reactions of birnessite at different current densities (Figure S8).

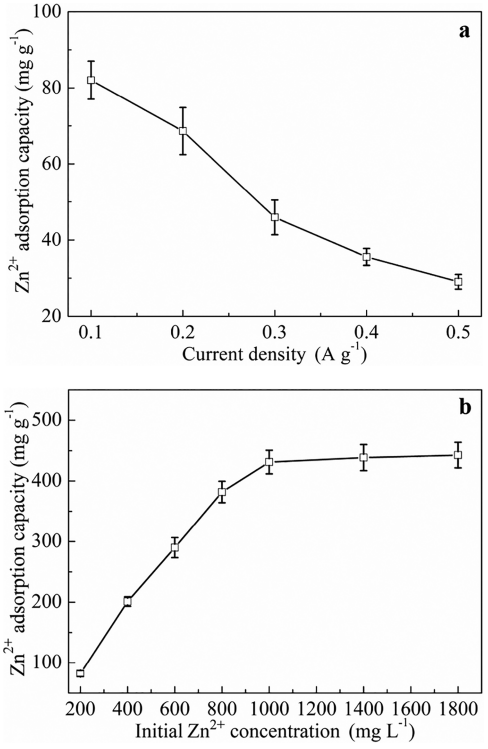

Figure 6. Zn^{2+} adsorption capacities of the birnessite electrodes after charge−discharge for 50 cycles in symmetric electrode system at different current densities in 200 mg L^{-1} Zn^{2+} solution (a) and in a three-electrode system of Zn^{2+} solutions at different concentrations (b).

The electrochemical adsorption for Zn^{2+} was performed in the three-electrode system to investigate the effect of electrochemical technique on Zn^{2+} adsorption capacity (Figure 6b). In 200 mg L^{-1} Zn^{2+} solution, the Zn^{2+} adsorption capacity of birnessite reached 82.0 mg g^{-1} (126.0 mmol mol^{-1}) and increased with the increase of Zn^{2+} concentration. In 1000 mg L^{-1} Zn^{2+} solution, the Zn^{2+} adsorption capacity reached the maximum of 442.6 mg g^{-1} (680.3 mmol mol^{-1}), and the corresponding maximum Mn^{2+} release reached 179.0 mg g^{-1} (Figure S9). In the end, the Zn/Mn molar ratio in the electrode was close to 1:1. Compared with those in the symmetric electrode system, the maximum Zn^{2+} adsorption capacity and Mn^{2+} release capacity in the three-electrode system were higher. The weaker XRD diffraction peak of (001) plane after electrochemical redox reactions indicated a higher degree of redox reaction in the three-electrode system (Figure S10).

DISCUSSION

Photochemical Formation Mechanism of Birnessite. As the precursor of many kinds of manganese oxides including cryptomelane and todorokite,[38] birnessite is widely present in various geological settings, such as surface coatings and crusts, terrestrial ore deposits and deep-sea nodules.[39,40] The formation and transformation of birnessite affect the geochemical cycling of some major nutrients and toxic elements.[38−40] To examine the existence of $OH^{\bullet}$ and $O_2^{\bullet-}$, BA and SOD were, respectively, added into the reaction of $NaNO_3$ (0.2 mmol L^{-1}) and $MnSO_4$ (0.1 mmol L^{-1}) with the initial pH of 6.0 under solar irradiation (Figure S11). After the addition of BA, the consumption of Mn^{2+}_{aq} decreased. No obvious consumption of Mn^{2+}_{aq} was observed in the reaction with SOD. These results indicate that the main oxidant is $O_2^{\bullet-}$ rather than $OH^{\bullet}$ during the photochemical reaction. The decrease in the consumption of Mn^{2+} after the addition of BA may be caused by the inhibition of the generation pathway of $O_2^{\bullet-}$.[41] The concentrations of Mn^{2+} and NO_3^- are low in natural environment. For example, the concentration of nitrate can reach up to 0.2 mmol L^{-1} in some eutrophic waters.[42] Birnessite nanosheets were also observed in the reaction of 0.1 mmol L^{-1} $MnSO_4$ and 0.2 mmol L^{-1} $NaNO_3$ with a constant pH of 6.0 under solar irradiation (Figure S12), indicating the possible photochemical formation of birnessite in natural environments.

In previous reports, hexagonal birnessite nanosheets could be obtained by the exfoliation of three-dimensional birnessite, which involves protonation, exfoliation, and self-assembly.[43,44] Here, the specific surface area of the hexagonal birnessite nanosheets formed through one-step photochemical reaction reached 179.0 m^2 g^{-1}. Large specific surface area and two-dimensional structure facilitate the rapid electrochemical reaction by providing more effective active sites.[7,19] Compared with traditional methods for the preparation of birnessite nanosheets, the photochemical method shows advantages of simple operation, energy saving, and environmental sustainability.

DOI: 10.1021/acssuschemeng.8b02191
ACS Sustainable Chem. Eng. 2018, 6, 13907−13914

Zinc Adsorption Mechanisms and Influencing Factors. The Zn^{2+} adsorption capacity of the birnessite nanosheets in the presence of electrochemical redox reactions was significantly higher than that at open circuit. In the electrochemical adsorption, the potential of the working and counter electrodes (vs SCE) varied within −0.1 and +0.8 V (Figure S13), and there were redox reactions of Mn(III) and Mn(IV).[8,45] In deionization capacitors, the ions are removed by electrostatic adsorption.[46,47] In deionization battery systems, the redox reactions of CuHCF electrodes facilitate the adsorption of salt ions.[48] In this work, the redox reactions of birnessite electrode were applied to improve Zn^{2+} adsorption capacity. The charge−discharge process of MnO_2 can be expressed as $MnO_2 + xM^+ + xe^- \rightleftharpoons MnOOM_x$ (M^+ is protons or alkali metal ions).[49] The insertion and extraction processes of M^+ are reversible due to its weak electrostatic action with manganese oxides, and thus $Na_4Mn_9O_{18}$ electrode material can be used for seawater desalination.[50] In the presence of heavy metal ions, inner-sphere complexes can be formed.[9] The adsorbed Zn^{2+} could not be fully released into the solution in the charge processes, resulting in the incomplete reversibility of redox reactions, as indicated by the asymmetrical redox peaks and cyclic voltammetry plots in the presence of Zn^{2+}. Accordingly, the adsorption capacity for Zn^{2+} can be enhanced through the not fully reversible redox reactions.

The not fully reversible redox reactions changed the Mn AOS and chemical composition of birnessite. In Mg/MnO_2 batteries, birnessite can be reduced to $MgMn_2O_4$ in the discharge processes.[51] In our previous work, the transformation of Mn_2O_3 nanoparticles to flower-like birnessite occurred in the charge−discharge processes of pseudocapacitors.[11] When the electrochemical reactions of flower-like birnessite were conducted in Zn^{2+} solution, $ZnMn_2O_4$ and Mn_3O_4 nanoparticles were observed during the constant-potential electrolysis process,[45] and Zn-buserite nanosheets were obtained during the charge−discharge process.[8] After electrochemical redox reactions, the Mn AOS of the birnessite decreased in this work (Figures 4 and 5). In addition, the release of Mn^{2+} could provide more vacancy sites, which may also lead to enhanced Zn^{2+} adsorption capacity of birnessite. During the discharge process, the birnessite could gain electrons, leading to the adsorption of Na^+, H^+ and Zn^{2+} on the electrode surface for charge balance. During the charge process, the adsorbed Na^+ and H^+ can be released into the solution due to good reversibility, while Zn^{2+} could be enriched on the electrode due to the not fully reversible redox reactions. Hence, the changes in the Mn AOS and chemical composition of birnessite facilitate the adsorption of Zn^{2+}.

The change in the micromorphology of birnessite also contributes to the electrochemical adsorption. During the electrochemical reactions of birnessite, redox reactions occur on the electrode surface.[8,49,52] Compared with constant potential electrolysis, cyclic redox process provides more adsorption sites and a better contact between the Zn^{2+} ion in the solution and birnessite inside the electrode by cyclically changing the micromorphology of the birnessite, which facilitates the electrochemical adsorption of Zn^{2+}.[8,45] The increase in the initial Zn^{2+} concentration contributed to the rapid redox reactions on the surface of birnessite electrode. Therefore, the increase of initial Zn^{2+} concentration may lead to the increase of adsorption sites and capacity.

In addition, the pH in the experiment was much higher than the point of zero charge of birnessite (~2 to 3).[9] The final pH of the solution increased with increasing initial Zn^{2+} concentration. Hence, the negative charge on the birnessite surface would increase with increasing initial Zn^{2+} concentration, which may also contribute to enhanced Zn^{2+} adsorption capacity with increasing initial Zn^{2+} concentration.[8]

In our previous work, the hierarchical birnessite obtained from the reduction of $KMnO_4$ was transformed into Zn-buserite and $ZnMn_2O_4$ after multicycle galvanostatic charge−discharge in Zn^{2+} solution. The XAFS results indicated that the Zn^{2+} was inserted into the interlayer and was adsorbed below or above the Mn(IV) vacancies of birnessite.[8] In this work, Zn-buserite and $ZnMn_2O_4$ were not observed. Thus, the Zn^{2+} was likely adsorbed below or above the Mn(IV) vacancies.[16] The Zn/Mn molar ratio reached about 1:1 in the electrode after electrochemical adsorption in the three-electrode system. We speculate that the Zn-rich manganese oxide may have the similar structure of quenselite ($Pb^{2+}Mn^{3+}O_2OH$) with the substitution of Pb^{2+} by Zn^{2+}.[6] Another possibility is that the MnO_6 octahedral layer is dioctahedral with the Mn vacancies capped on each side by Zn, which is similar to the structure of gibbsite.[53] In this case, the stoichiometry would be $ZnMn^{3+/4+}O_{2-x}$. Hence, the Zn^{2+} adsorption capacity may also be improved by adjusting the arrangement of MnO_6 octahedra during the electrochemical redox reactions.

The Zn^{2+} adsorption capacity of birnessite electrode decreased with increasing current density. During charge−discharge, the redox reactions of birnessite occur mainly on the surface of electrode.[8,49,52] Due to the diffusion limit of Na^+, the electrochemical specific capacitance of birnessite electrode decreases with increasing current density in the supercapacitors.[52] The same change of electrochemical specific capacitance was observed in this work (Figure S6). Hence, we speculate that the diffusion of Zn^{2+} or Na^+ limits the rate of electrochemical reactions at high current density.

Compared with that in the symmetric electrode system, the higher degree of redox reactions and release of Mn^{2+} in the three-electrode system lead to higher Zn^{2+} adsorption capacity of birnessite (Figures 3 and 6b). However, the Mn^{2+} release capacity was also higher in the three-electrode system (Figures S3 and S7b). Under the condition of maximum adsorption capacity, the Zn^{2+} adsorption amounts corresponding to per unit of Mn^{2+} release were, respectively, 3.42, 2.47, and 0.58 mg mg^{-1} in the symmetric electrode system, the three-electrode system, and at open circuit. Thus, the symmetric electrode system has an advantage in reducing the Mn^{2+} release capacity.

During the heavy metal ion removal, energy consumption is also a big challenge for membrane filtration and some traditional electrochemical processes including electrodeposition and electrocoagulation.[5] After charge−discharge for 50 cycles in symmetric electrode system, the Coulombic efficiency of birnessite electrode reached about 100% at different current densities (Figure S6). The electric power was consumed and transformed into chemical energy during the charge process. We can obtain the electric power during the discharge processes, which is accompanied by the Zn^{2+} adsorption on manganese oxides. Therefore, the electrochemical adsorption system driven by electrochemical redox reactions could also be used as a supercapacitor for power storage.

DOI: 10.1021/acssuschemeng.8b02191
ACS Sustainable Chem. Eng. 2018, 6, 13907−13914

CONCLUSIONS

Two-dimensional birnessite nanosheets were readily synthesized through the photochemical reaction of NO_3^- and Mn^{2+}_{aq} under solar irradiation. The Zn^{2+} adsorption capacity of the as-obtained birnessite can be enhanced by electrochemical redox reactions due to the changes in Mn AOS, surface properties, and chemical compositions. With increasing current density, the Zn^{2+} adsorption capacity decreases. Compared with that in the symmetric electrode system, the highest Zn^{2+} adsorption capacity in the three-electrode system is higher. However, the symmetric electrode system has an advantage in reducing the Mn^{2+} release capacity. In this work, the method for the preparation of birnessite under solar irradiation is "green" and sustainable, and the system for heavy metal ion removal driven by electrochemical redox reactions could also be used as a supercapacitor for power storage.

ASSOCIATED CONTENT

Supporting Information

The Supporting Information is available free of charge on the ACS Publications website at DOI: 10.1021/acssuschemeng.8b02191.

Supporting methods, adsorption capacities of different materials, Mn AOS obtained from XANES, FT-IR spectrum, N_2 adsorption−desorption isotherm and pore size distribution of birnessite, released Mn^{2+}, XRD patterns, FESEM images, electrochemical specific capacitance and potential of birnessite electrodes, and Mn^{2+} concentration in the photochemical reaction (PDF)

AUTHOR INFORMATION

Corresponding Author

*E-mail: qiugh@mail.hzau.edu.cn. Tel.: +86(0)27 87280271.

ORCID

Wenfeng Tan: 0000-0002-3098-2928
Steven L. Suib: 0000-0003-3073-311X
Guohong Qiu: 0000-0002-1181-3707
Qiaoyun Huang: 0000-0002-2733-8066

Notes

The authors declare no competing financial interest.

ACKNOWLEDGMENTS

We acknowledge the support from the National Natural Science Foundation of China (Grant Nos. 41571228, 41425006, and 41877025), the National Key Research and Development Program of China (Grant Nos. 2017YFD0801000 and 2018YFD0800304), the Fundamental Research Funds for the Central Universities (Program Nos. 2662018JC055 and 2662015JQ002), and the Fok Ying-Tong Education Foundation (Grant No. 141024). S.L.S. thanks the U.S. Department of Energy, Office of Basic Energy Sciences, Division of Chemical, Biological and Geological Sciences for support under Grant DE-FG02-86ER13622.A000. The authors are grateful to Prof. Dr. T. David Waite at The University of New South Wales for technical discussions, Dr. Shengqi Chu at Beijing Synchrotron Radiation Facility for the XANES data collection, and Dr. Jianbo Cao and Dr. Lihong Qin at Public Laboratory of Electron Microscope of Huazhong Agricultural University for TEM and SEM technical support.

REFERENCES

(1) Fu, F. L.; Wang, Q. Removal of heavy metal ions from wastewaters: A review. *J. Environ. Manage.* **2011**, *92* (3), 407−418.

(2) Zhou, G. Y.; Luo, J. M.; Liu, C. B.; Chu, L.; Ma, J. H.; Tang, Y. H.; Zeng, Z. B.; Luo, S. L. A highly efficient polyampholyte hydrogel sorbent based fixed-bed process for heavy metal removal in actual industrial effluent. *Water Res.* **2016**, *89*, 151−160.

(3) Wang, H.; Yuan, X. Z.; Wu, Y.; Huang, H. J.; Zeng, G. M.; Liu, Y.; Wang, X. L.; Lin, N. B.; Qi, Y. Adsorption characteristics and behaviors of graphene oxide for Zn(II) removal from aqueous solution. *Appl. Surf. Sci.* **2013**, *279* (8), 432−440.

(4) Chibuike, G. U.; Obiora, S. C. Heavy metal polluted soils: Effect on plants and bioremediation methods. *Appl. Environ. Soil Sci.* **2014**, *2014*, 1−12.

(5) Huang, Z.; Lu, L.; Cai, Z. X.; Ren, Z. J. Individual and competitive removal of heavy metals using capacitive deionization. *J. Hazard. Mater.* **2016**, *302* (3), 323−31.

(6) Manceau, A.; Lanson, B.; Drits, V. A. Structure of heavy metal sorbed birnessite. Part III: Results from powder and polarized extended X-ray absorption fine structure spectroscopy. *Geochim. Cosmochim. Acta* **2002**, *66* (15), 2639−2663.

(7) Liu, J. T.; Ge, X.; Ye, X. X.; Wang, G. Z.; Zhang, H. M.; Zhou, H. J.; Zhang, Y. X.; Zhao, H. J. 3D graphene/δ-MnO_2 aerogels for highly efficient and reversible removal of heavy metal ions. *J. Mater. Chem. A* **2016**, *4* (5), 1970−1979.

(8) Liu, L. H.; Luo, Y.; Tan, W. F.; Liu, F.; Suib, S. L.; Zhang, Y. S.; Qiu, G. H. Zinc removal from aqueous solution using a deionization pseudocapacitor with a high-performance nanostructured birnessite electrode. *Environ. Sci.: Nano* **2017**, *4* (4), 811−823.

(9) Feng, X. H.; Zhai, L. M.; Tan, W. F.; Liu, F.; He, J. Z. Adsorption and redox reactions of heavy metals on synthesized Mn oxide minerals. *Environ. Pollut.* **2007**, *147* (2), 366−373.

(10) Wang, Y.; Feng, X. H.; Villalobos, M.; Tan, W. F.; Liu, F. Sorption behavior of heavy metals on birnessite: Relationship with its Mn average oxidation state and implications for types of sorption sites. *Chem. Geol.* **2012**, *292−293* (1), 25−34.

(11) Chen, S. L.; Liu, F.; Xiang, Q. J.; Feng, X. H.; Qiu, G. H. Synthesis of Mn_2O_3 microstructures and their energy storage ability studies. *Electrochim. Acta* **2013**, *106*, 360−371.

(12) Chen, B. W.; Wang, Y. F.; Chang, Z.; Wang, X. W.; Li, M. X.; Liu, X.; Zhang, L. X.; Wu, Y. P. Enhanced capacitive desalination of MnO_2 by forming composite with multi-walled carbon nanotubes. *RSC Adv.* **2016**, *6* (8), 6730−6736.

(13) El-Deen, A. G.; Barakat, N. A. M.; Kim, H. Y. Graphene wrapped MnO_2-nanostructures as effective and stable electrode materials for capacitive deionization desalination technology. *Desalination* **2014**, *344*, 289−298.

(14) Hu, C. Z.; Liu, F. Y.; Lan, H. C.; Liu, H. J.; Qu, J. H. Preparation of a manganese dioxide/carbon fiber electrode for electrosorptive removal of copper ions from water. *J. Colloid Interface Sci.* **2015**, *446*, 359−365.

(15) Kwon, K. D.; Refson, K.; Sposito, G. Understanding the trends in transition metal sorption by vacancy sites in birnessite. *Geochim. Cosmochim. Acta* **2013**, *101* (2), 222−232.

(16) Silvester, E.; Manceau, A.; Drits, V. A. Structure of synthetic monoclinic Na-rich birnessite and hexagonal birnessite: II. Results from chemical studies and EXAFS spectroscopy. *Am. Mineral.* **1997**, *82* (9−10), 962−978.

(17) Peng, Q. C.; Liu, L. H.; Luo, Y.; Zhang, Y. S.; Tan, W. F.; Liu, F.; Suib, S. L.; Qiu, G. H. Cadmium removal from aqueous solution by a deionization supercapacitor with a birnessite electrode. *ACS Appl. Mater. Interfaces* **2016**, *8* (50), 34405−34413.

(18) Marafatto, F. F.; Lanson, B.; Peña, J. Crystal growth and aggregation in suspensions of δ-MnO_2 nanoparticles: implications for surface reactivity. *Environ. Sci.: Nano* **2018**, *5* (2), 497−508.

(19) Huang, M.; Zhang, Y. X.; Li, F.; Zhang, L. L.; Ruoff, R. S.; Wen, Z. Y.; Liu, Q. Self-Assembly of mesoporous nanotubes assembled from interwoven ultrathin birnessite-type MnO_2 nanosheets for asymmetric supercapacitors. *Sci. Rep.* **2014**, *4*, 3878.

DOI: 10.1021/acssuschemeng.8b02191
ACS Sustainable Chem. Eng. 2018, 6, 13907−13914

(20) Jung, H.; Chadha, T. S.; Kim, D.; Biswas, P.; Jun, Y.-S. Photochemically assisted fast abiotic oxidation of manganese and formation of δ-MnO_2 nanosheets in nitrate solution. *Chem. Commun.* **2017**, *53* (32), 4445−4448.
(21) Kärkäs, M. D.; Porco, J. A.; Stephenson, C. R. J. Photochemical approaches to complex chemotypes: Applications in natural product synthesis. *Chem. Rev.* **2016**, *116* (17), 9683−9747.
(22) Oelgemöller, M. Solar photochemical synthesis: From the beginnings of organic photochemistry to the solar manufacturing of commodity chemicals. *Chem. Rev.* **2016**, *116* (17), 9664−9682.
(23) Buxton, G. V.; Greenstock, C. L.; Helman, W. P.; Ross, A. B. Critical review of rate constants for reactions of hydrated electrons, hydrogen atoms and hydroxyl radicals ($\cdot OH/\cdot O^-$ in Aqueous Solution. *J. Phys. Chem. Ref. Data* **1988**, *17* (2), 513−886.
(24) Scharko, N. K.; Berke, A. E.; Raff, J. D. Release of nitrous acid and nitrogen dioxide from nitrate photolysis in acidic aqueous solutions. *Environ. Sci. Technol.* **2014**, *48* (20), 11991−12001.
(25) Liu, L. H.; Jia, Z. H.; Tan, W. F.; Suib, S. L.; Ge, L.; Qiu, G. H.; Hu, R. G. Abiotic photomineralization and transformation of iron oxide nanominerals in aqueous systems. *Environ. Sci.: Nano* **2018**, *5* (5), 1169−1178.
(26) Zhao, Y.; Meng, Y. N.; Jiang, P. Carbon@MnO_2 core−shell nanospheres for flexible high-performance supercapacitor electrode materials. *J. Power Sources* **2014**, *259* (7), 219−226.
(27) Lim, J.; Lee, J. M.; Park, B.; Jin, X. Y.; Hwang, S.-J. Homogeneous cationic substitution for two-dimensional layered metal oxide nanosheets *via* a galvanic exchange reaction. *Nanoscale* **2017**, *9* (2), 792−801.
(28) Joo, S. H.; Feitz, A. J.; Sedlak, D. L.; Waite, T. D. Quantification of the oxidizing capacity of nanoparticulate zero-valent iron. *Environ. Sci. Technol.* **2005**, *39* (5), 1263−1268.
(29) Drits, V. A.; Silvester, E. S.; Gorshkov, A. I.; Manceau, A. Structure of synthetic monoclinic Na-rich birnessite and hexagonal birnessite: I. Results from X-ray diffraction and selected-area electron diffraction. *Am. Mineral.* **1997**, *82*, 946−961.
(30) Grangeon, S.; Lanson, B.; Miyata, N.; Tani, Y.; Manceau, A. Structure of nanocrystalline phyllomanganates produced by fresh-water fungi. *Am. Mineral.* **2010**, *95* (11−12), 1608−1616.
(31) Post, J. E.; Veblen, D. R. Crystal structure determinations of synthetic sodium, magnesium, and potassium birnessite using TEM and the Rietveld method. *Am. Mineral.* **1990**, *75* (5−6), 477−489.
(32) Alfaruqi, M. H.; Mathew, V.; Gim, J.; Kim, S.; Song, J. J.; Baboo, J. P.; Choi, S. H.; Kim, J. Electrochemically induced structural transformation in a γ-MnO_2 cathode of a high capacity zinc-ion battery system. *Chem. Mater.* **2015**, *27* (10), 3609−3620.
(33) Pan, H. L.; Shao, Y. Y.; Yan, P. F.; Cheng, Y. W.; Han, K. S.; Nie, Z. M.; Wang, C. M.; Yang, J. H.; Li, X. L.; Bhattacharya, P.; Mueller, K. T.; Liu, J. Reversible aqueous zinc/manganese oxide energy storage from conversion reactions. *Nat. Energy* **2016**, *1*, 16039.
(34) Zhao, W.; Wang, Q. Q.; Liu, F.; Qiu, G. H.; Tan, W. F.; Feng, X. H. Pb^{2+} adsorption on birnessite affected by Zn^{2+} and Mn^{2+} pretreatments. *J. Soils Sediments* **2010**, *10* (5), 870−878.
(35) Zhao, W.; Cui, H. J.; Liu, F.; Tan, W. F.; Feng, X. H. Relationship between Pb^{2+} adsorption and average Mn oxidation state in synthetic birnessites. *Clays Clay Miner.* **2009**, *57* (5), 513−520.
(36) Bailey, S. W. The status of clay mineral structures. *Clays Clay Miner.* **1966**, *14* (5), 1−23.
(37) Manceau, A.; Marcus, M. A.; Grangeon, S. Determination of Mn valence states in mixed-valent manganates by XANES spectroscopy. *Am. Mineral.* **2012**, *97* (5−6), 816−827.
(38) Bodeï, S.; Manceau, A.; Geoffroy, N.; Baronnet, A.; Buatier, M. Formation of todorokite from vernadite in Ni-rich hemipelagic sediments. *Geochim. Cosmochim. Acta* **2007**, *71* (23), 5698−5716.
(39) Manceau, A.; Kersten, M.; Marcus, M. A.; Geoffroy, N.; Granina, L. Ba and Ni speciation in a nodule of binary Mn oxide phase composition from Lake Baikal. *Geochim. Cosmochim. Acta* **2007**, *71* (23), 1967−1981.
(40) Manceau, A.; Lanson, M.; Takahashi, Y. Mineralogy and crystal chemistry of Mn, Fe, Co, Ni, and Cu in a deep-sea Pacific polymetallic nodule. *Am. Mineral.* **2014**, *99* (10), 2068−2083.
(41) Mack, J.; Bolton, J. R. Photochemistry of nitrite and nitrate in aqueous solution: a review. *J. Photochem. Photobiol., A* **1999**, *128* (1), 1−13.
(42) Xu, H.; Paerl, H. W.; Qin, B. Q.; Zhu, G. W.; Gao, G. Nitrogen and phosphorus inputs control phytoplankton growth in eutrophic Lake Taihu, China. *Limnol. Oceanogr.* **2010**, *55* (1), 420−432.
(43) Ma, R. Z.; Sasaki, T. Two-Dimensional oxide and hydroxide nanosheets: Controllable high-quality exfoliation, molecular assembly, and exploration of functionality. *Acc. Chem. Res.* **2015**, *48* (1), 136−143.
(44) Yang, X. J.; Makita, Y.; Liu, Z.-H.; Sakane, K.; Ooi, K. Structural characterization of self-assembled MnO_2 nanosheets from birnessite manganese oxide single crystals. *Chem. Mater.* **2004**, *16* (26), 5581−5588.
(45) Liu, L. H.; Qiu, G. H.; Suib, S. L.; Liu, F.; Zheng, L. R.; Tan, W. F.; Qin, L. H. Enhancement of Zn^{2+} and Ni^{2+} removal performance using a deionization pseudocapacitor with nanostructured birnessite and its carbon nanotube composite electrodes. *Chem. Eng. J.* **2017**, *328*, 464−473.
(46) Tang, W. W.; Kovalsky, P.; Cao, B. C.; He, D.; Waite, T. D. Fluoride removal from brackish groundwaters by constant current capacitive deionization (CDI). *Environ. Sci. Technol.* **2016**, *50* (19), 10570−10579.
(47) Tang, W. W.; He, D.; Zhang, C. Y.; Waite, T. D. Optimization of sulfate removal from brackish water by membrane capacitive deionization (MCDI). *Water Res.* **2017**, *121*, 302−310.
(48) Kim, T.; Gorski, C. A.; Logan, B. E. Low energy desalination using battery electrode deionization. *Environ. Sci. Technol. Lett.* **2017**, *4* (10), 444−449.
(49) Simon, P.; Gogotsi, Y. Materials for electrochemical capacitors. *Nat. Mater.* **2008**, *7* (11), 845−854.
(50) Lee, J.; Kim, S.; Kim, C.; Yoon, J. Hybrid capacitive deionization to enhance the desalination performance of capacitive techniques. *Energy Environ. Sci.* **2014**, *7*, 3683−3689.
(51) Sun, X. Q.; Duffort, V.; Mehdi, B. L.; Browning, N. D.; Nazar, L. F. Investigation of the mechanism of Mg insertion in birnessite in nonaqueous and aqueous rechargeable Mg-ion batteries. *Chem. Mater.* **2016**, *28* (2), 534−542.
(52) Liu, L. H.; Luo, Y.; Tan, W. F.; Zhang, Y. S.; Liu, F.; Qiu, G. H. Facile synthesis of birnessite-type manganese oxide nanoparticles as supercapacitor electrode materials. *J. Colloid Interface Sci.* **2016**, *482*, 183−192.
(53) Manceau, A.; Marcus, M. A.; Tamura, N.; Proux, O.; Geoffroy, N.; Lanson, B. Natural speciation of Zn at the micrometer scale in a clayey soil using X-ray fluorescence, absorption, and diffraction. *Geochim. Cosmochim. Acta* **2004**, *68* (11), 2467−2483.

DOI: 10.1021/acssuschemeng.8b02191
ACS Sustainable Chem. Eng. 2018, 6, 13907−13914